Power Electronic Devices and Components 3 (2022) 100016

Contents lists available at ScienceDirect

Power Electronic Devices and Components

journal homepage: www.journals.elsevier.com/power-electronic-devices-and-components

Input and output total currents characterization in *BCM* and *CCM* Interleaved Power Converters Under Inductance Mismatch

Paula Cervellini [*,a], Marco Carnaghi [a], Pablo Antoszczuk [a], Rogelio García Retegui [a], Marcos Funes [a]

Universidad Nacional de Mar del Plata, J.B.Justo 4302, Mar del Plata, Buenos Aires 7600, Argentina

ARTICLE INFO

Keywords:
Interleaved power converters
Inductance mismatch
Continuous Conduction Mode (*CCM*)
Boundary Conduction Mode (*BCM*)
Total input current
Total output current

ABSTRACT

This paper presents a complete characterization of input and output currents in interleaved power converters with inductance mismatch, operating in Boundary Conduction Mode (*BCM*) and Continuous Conduction Mode (*CCM*). The proposal allows to compute these currents in several interleaved converter topologies for the entire range of operating points, considering any number of phases and any inductance ratio. Input and output currents are recovered from the values obtained when adding the phase currents in the instants where the slopes change; values that are thus defined as key points. This methodology is based on the coincidences that exist between the instants of the phase current key points and those of total currents. By using the computed key points, ripple amplitude, rms value and harmonic content of input and output total currents for the entire range of operating points can be easily obtained. Simulations are conducted on a 5-phase boost converter and a 5-phase buck converter under different conditions in order to validate the proposal expressions. Experimental tests on a 5-phase buck converter are presented under different operation conditions to verify that the proposed method can be applied in real situation.

1. Introduction

The importance of characterizing and analyzing input and output currents in dc-dc converters is well stated in the literature, as they impact not only on the performance of the components and devices connected to the converter but also on the filters design, the thermal stress, the electromagnetic interferences and the converter losses, among others Huangfu et al. (2021), Kjaer et al. (2005), Schuck and Pilawa-Podgurski (2015), Valdez-Resendiz et al. (2018). In this sense, characterization is even more important and complex when multiphase converters are considered. This converters result from the parallel association of N equal converters named phases. Fig. 1 shows the structure of a 4-phase boost converter operating in CCM with all converters connected to a V_{in} input voltage and a V_{out} output voltage. It also presents inductor total current (i_L) inductor phase currents (i_{L_k}) and the respective switch command signals (PWM_k). A commonly used control technique in this converters is called interleaved and consists in equally phase-shifting the switching instants within a switching period as shown in the *PWM* waveforms of Fig. 1. Advantages of interleaved power converters include reduction of the total current ripple amplitude and increase of its frequency to N times the switching frequency (f_{sw}) as evidenced in Fig. 1.

Aforementioned advantages are disrupted under phase inductance mismatch. This means that f_{sw} component and its first $N-1$ harmonics are no longer canceled and the amplitude is not reduced in the same amount whenever differences between the inductors exist Antoszczuk et al. (2014); Farahani et al. (2020); Foley et al. (2012); Nouri et al. (2013) as evidenced in Fig. 2. What is more, the dependence of current characteristics of N, f_{sw}, the operating point and the switching sequence makes it difficult to obtain a general closed expression to determine total current Garc-a et al. (2007). In this sense, in the design process, an oversizing of converter components and input and output filtering stages is necessary so as to meet the application requirements Johnson and Krein (2017).

Hence, the knowledge of any of total current characteristics is important for the evaluation and optimization of converter designs Farahani et al. (2020); Gupta and Patra (2005); Liu et al. (2021); Mihajlovic and and (2004); Rodriguez et al. (2012); Seyezhai and Mathur (2012); Slah et al. (2017); Tsolaridis et al. (2021); Wang et al. (2019), the design of ripple optimization algorithms Antoszczuk et al. (2017); Schuck and Pilawa-Podgurski (2015), and the assessment of losses and temperature rise in the components connected to the

* Corresponding author.

https://doi.org/10.1016/j.pedc.2022.100016
Received 21 March 2022; Received in revised form 14 July 2022; Accepted 3 August 2022
Available online 5 August 2022

converter Galigekere and Kazimierczuk (2012); Karatzaferis et al. (2017); Liu et al. (2017).

Many attempts have been made in the literature to characterize total current, but only for particular cases, such as certain number of phases, specific converter topologies, particular operating points or inductance ratios Abu-Qahouq et al. (2007); Garc-a et al. (2007); Gu and Zhang (2013); Huber et al. (2008). In previous work Antoszczuk et al. (2014) a *CCM* ripple characterization for any number of phases and any inductance ratio was accomplished. However, it can only characterize inductor current ripple, which means that can only compute boost converter input current ripple or buck converter output current ripple. Afterwards, in Cervellini et al. (2020), a complete input and output current characterization of several topologies of interleaved converters operating in *DCM* for any number of phases *N*, any inductance ratio and for the entire range of operating points was assessed. Therefore, in order to obtain a complete input and output current characterization of interleaved power converters operating in *BCM* and *CCM* modes, as the one presented for *DCM* operation, a similar approach as the presented in Cervellini et al. (2020) must be considered, but with the inherent complexity of *BCM* and *CCM* current waveforms.

The proposed methodology obtains the input and output total current for many converter topologies by summing the contribution of each phase in certain key points. In this sense, a general representation that is evaluated to obtain the different types of input and output phase currents, is presented. Subsequently, using computed total current values, ripple amplitude, rms value and harmonic content are obtained. In order to validate the expressions obtained for each type of current, the calculations are compared to simulation results of both 5-phase boost and buck converters. Additionally, experimental tests on a 5-phase buck converter are presented to verify that the proposed method can be applied in real situation.

The main contributions of this paper are:

- A general waveform, that allows to derive inductor, switch and diode phase current waveforms.
- The recovery of input and output total currents obtained from discrete values (key points), by adding the phase currents in the instants where the slopes change.
- A complete characterization of total input and output currents for several power converter topologies.
- The computation of input and output total currents characteristics such as ripple amplitude, rms value and harmonic content from the key points, for the entire range of duty cycles and any number of phases.

2. Proposed current characterization

The proposed method is based on the analysis of the geometry of each phase and the selective sum of the phases value in certain key points. As *BCM* is a particular case of *CCM* operation, the analysis is presented for *CCM* condition.

With the aim of conducting the analysis, some considerations are taken into account. Firstly, it is considered that the converter is operating in steady-state condition. Secondly, as the inductors time constant (given by the inductance and its resistive component) is much larger than *T*, current is approximated by linear segments Antoszczuk (2016). Additionally, the switching period (*T*) of all *N* phases can be considered equal due to the accuracy of modern digital platforms Monmasson et al. (2011). Moreover, the phase shift of current ripples is assumed as $T_n = \frac{T}{N}$ by means of digital control (García et al., 2006).

Above considerations allow to approximate the input and output phase current ripples as a piecewise linear function with different slopes that change in time instants defined as key points. In this sense, total input or output current also result in a waveform composed by linear segments with different slopes and duration, in which key points agree with the key points in each phase current ripple. Fig. 3 shows the input phase (i_k) and total (i_T) current for a boost *N*-phase *CCM* converter under inductance mismatch. In this figure, a generic key point for total current, p_x, is pointed out for the time instant t_x.

Therefore, the first step in order to characterize total current is to compute the location of the key points. Once all key points are located (t_x), total current for t_x instant (p_x) can be computed as the sum of phase currents in that instant $i_k(t_x)$ as (1).

$$p_x = i_1(t_x) + \cdots + i_k(t_x) + \cdots + i_N(t_x) = \sum_{k=1}^{N} i_k(t_x) \tag{1}$$

Input and output phase currents in different converters can be classified as inductor i_{L_k}, switch i_{S_k} and diode i_{D_k} currents, as shown in Fig. 4 for a 4-phase boost converter. The same occurs for buck and buck-boost converters, among others. Then, total input and output currents for many topologies can be characterized by computing the corresponding phase current key points and their respective values.

In order to present a general methodology to obtain the required variables, the waveform shown in Fig. 5 is proposed. By properly evaluating the different time intervals, inductor, switch and diode phase current waveforms may be derived as it considers the key points of each type of current. The proposed general waveform is a function of time *t*, inductor phase ripple amplitude A_k and inductor phase mean current I_{L_k} ($f(t, A_k, I_{L_k})$). Moreover it is a four-section function with five key points,

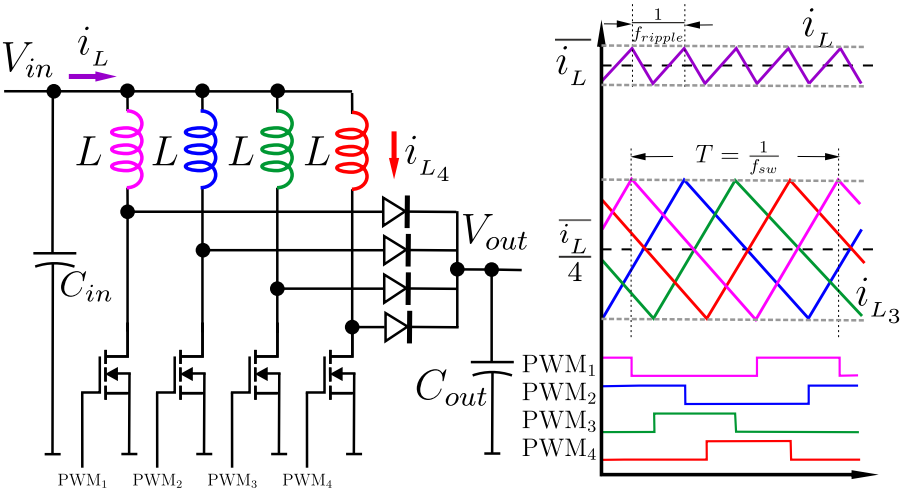

Fig. 1. 4-phase interleaved boost converter.

but, as it represents a periodic waveform, it has four key points per period: t_{up}, t_{on}, t_f and t_{down}. In the figure, T_{on} is the switch turned on time and T_f the switch turned off time. To represent the diode and switch abrupt changes in current, T_{on_e} and T_{f_e} infinitesimal time intervals are defined, thus obtaining T_{on_c} and T_{f_c} as shown in (2).

$$T = T_{on} + T_f \qquad T_{on} = T_{on_e} + T_{on_c} \qquad T_f = T_{f_e} + T_{f_c} \tag{2}$$

Interval T_f can be calculated as a function of T and T_{on}, and amplitude A_k as a function of T_{on} or T_f and phase current positive or negative slopes (s_{p_k} and s_{n_k}, respectively) as:

$$T_f = T - T_{on}\,; \quad A_k = T_{on_c} s_{p_k} = T_{f_c} s_{n_k} \tag{3}$$

where s_{p_k} and s_{n_k} computation is based on the topology parameters L_k, V_{in} and V_{out} Cervellini et al. (2020). Additionally, every point is delayed $T_n = T/N$ from the same point in the adjacent phase. Then, key points for any current and for phase k, considering $k = 1 : N$, can be computed as:

$$t_{up}(k) = (1-k)T_n \qquad t_{on}(k) = t_{up}(k) + T_{on_e} \tag{4}$$

$$t_f(k) = t_{on}(k) + T_{on_c} \qquad t_{down}(k) = t_f(k) + T_{f_c} \tag{5}$$

Therefore total current key points location is obtained as:

$$t_x = sort\left(\begin{bmatrix} t_{up} & t_{on} & t_f & t_{down} \end{bmatrix}\right) \tag{6}$$

where sort is a function that puts in order the time instants.

As the points of interest are the key points, the required information of the phase current ($i_k(t_x)$)) is obtained by computing $f(t, A_k, I_{L_k})$ in t_x instants and evaluating the proper A_k and I_{L_k} for the k^{th} phase. Then,

$$i_k(t_x) = f\left(t_x, A_k, I_{L_k}\right) \tag{7}$$

To compute $f(t, A_k, I_{L_k})$ value for each t_x the linear segments of the waveform are defined in Fig. 6, with a_1, a_2, a_3 and a_4 as the intercepts and b_1, b_2, b_3 and b_4 the slopes of the linear functions.

To obtain the slope and intercepts of the different currents, f_l, f_s and f_d boolean indicators are introduced in the equations and the logic operator or (||) is used. This indicators can take the value 0 or 1, depending the current that is being characterized.

Finally, the value of total current in t_x instants is obtained by summing the contribution of all phases in each singular point as shown in (8), where subindex z allows to determine which key point of i_k contributes to that instant in total current.

$$p_x = \sum_{k=1}^{N} i_k(t_z), \quad z = \begin{cases} x - 4k + 4 & \text{if } x > 4k-4 \\ x - 4k + 4(N+1) & \text{if } x \le 4k-4 \end{cases} \tag{8}$$

To compute total inductor current (p_{L_x}), total switch current (p_{S_x}) and total diode current (p_{D_x}) for t_x instants, $f(t, A_k, I_{L_k})$ function for each type of phase current must be calculated. Then, $f_L(t, A_k, I_{L_k})$ is defined for inductor phase current, $f_s(t, A_k, I_{L_k})$ for switch phase current and $f_D(t, A_k, I_{L_k})$ for diode phase current. Therefore T_{on_e}, T_{on_c}, T_{f_e} and T_{f_c} instants are properly evaluated taking into consideration that they can take the infinitesimal value T_i that stands for the current rising and falling times. Then, evaluating f_l, f_s and f_d indicators in $f(t, A_k, I_{L_k})$ as presented in Table 1, $f_L(t, A_k, I_{L_k})$, $f_S(t, A_k, I_{L_k})$ and $f_D(t, A_k, I_{L_k})$ functions and their corresponding key points are obtained.

In order to summarize the methodology, Fig. 7 shows a flow chart of the characterization procedure.

As previously mentioned, *BCM* operation represents a particular case of *CCM* since it takes place when A_k is equal to $2I_{L_k}$, then total input and output current for *BCM* is obtained by properly evaluating phase ripple amplitude and mean inductor current.

3. Total current characteristics calculation

This section introduces the computation of some characteristics of total currents i_{L_T}, i_{D_T} and i_{S_T}, taking into account the previous representation of these currents as piecewise functions.

3.1. Ripple amplitude

Total current ripple peak-to-peak amplitude Δi_{L_T} is calculated by subtracting the maximum and minimum values of the key points of total current.

In converters without inductance mismatch it can be observed that cancellation of current ripple ($\Delta i_{L_T} = 0$) is obtained for certain operating points. This situation occurs when there is superposition of segments with positive and negative slopes and coincident key points as represented in Fig. 8.

As, it can be seen from the figure, for a converter with $N = 3$, two superposition cases occur.

Then, in a converter with N phases $N-1$ superposition cases occur. By analyzing the different superposition cases, the values of $D = T_{on}/T$ that bring out total ripple cancellation are obtained as:

$$D_N = \frac{i}{N} \qquad i = 1 : (N-1) \tag{9}$$

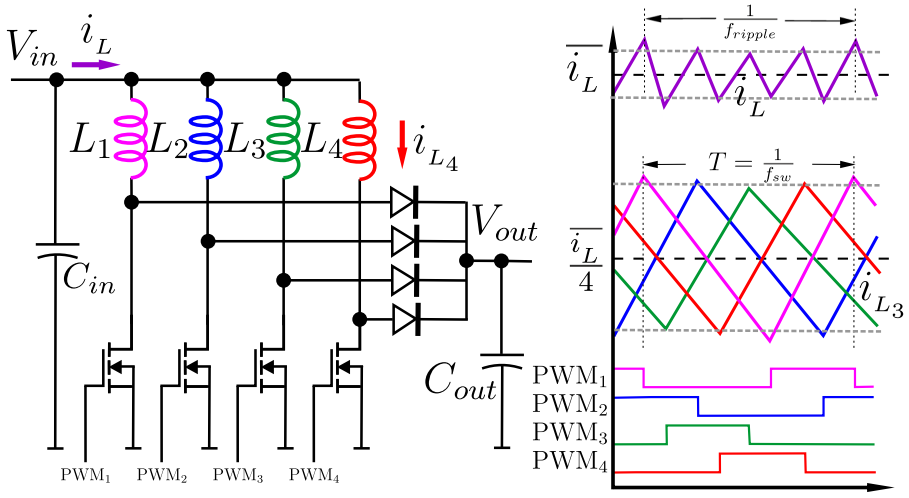

Fig. 2. 4-phase interleaved boost converter with inductance mismatch.

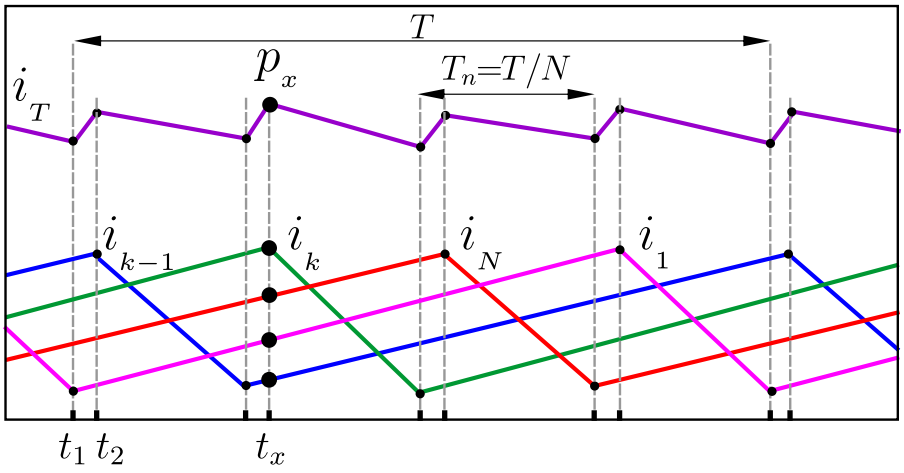

Fig. 3. Phase (i_k) and total (i_T) currents.

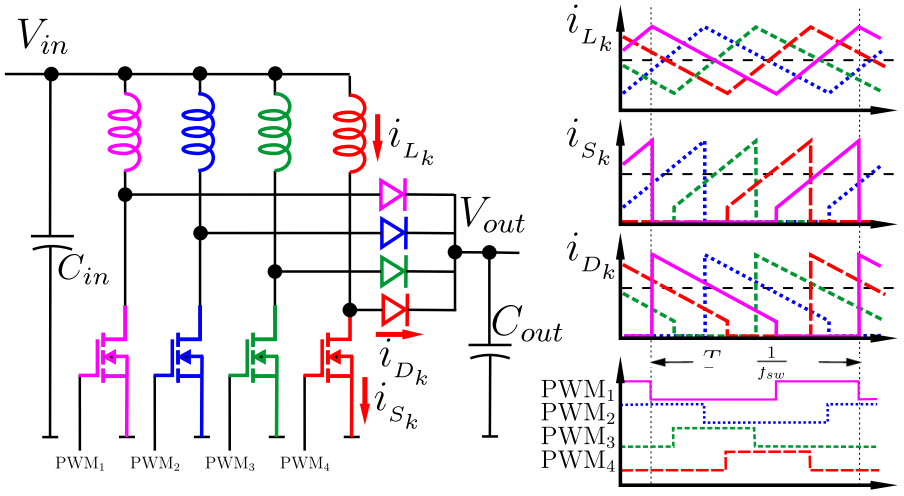

Fig. 4. Phase currents of a 4-phase interleaved boost converter.

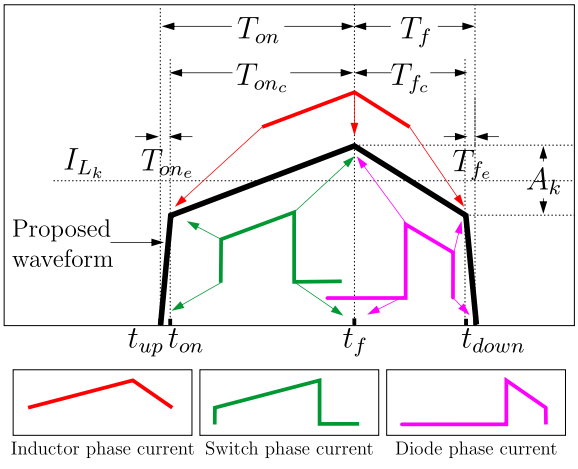

Fig. 5. Proposed general waveform.

For the case of practical converters, inductance mismatch generates differences in the value of the phase ripples slopes. For this reason no ripple cancellation is possible and local minimums are found instead, as it is demonstrated in Antoszczuk et al. (2014).

Regarding i_{s_T} and i_{D_T}, it is determined that no nulls or local minimums exist, as superposition of different sign slopes is not possible.

3.2. Rms value

The evaluation of input and output total current rms value is of interest when it is necessary to design Liu et al. (2017) or compute losses in filtering capacitors for the converter entire operation range Karatzaferis et al. (2017). Total rms value (i_{rms}) and ac rms value ($\tilde{i}_{rms}$) can be obtained from p_x and t_x as:

$$i_{rms} = \sqrt{\frac{1}{T}\left[\sum_{x=1}^{M}\int_{t_x}^{t_{x+1}} s(\tau)^2 d\tau\right]} \tag{10}$$

$$\tilde{i}_{rms} = \sqrt{{i_{rms}}^2 - {I_{L_k}}^2} \tag{11}$$

where M is the number of key points ($4N$) and $s(\tau) = m_x\tau + q_x$ is the linear equation of a given segment, whose slope and intercept are computed from the key points value and location as:

$$m_x = \frac{p_{x+1} - p_x}{t_{x+1} - t_x} \qquad q_x = p_x - t_x m_x \tag{12}$$

where p_x is obtained using (8). Replacing (12) in (10) i_{rms} is:

$$f(t) = \begin{cases} \mathbf{a_1} + \mathbf{b_1}t & 0 \le t < T_{on_e} \\ \mathbf{a_2} + \mathbf{b_2}t & T_{on_e} \le t < T_{on} \\ \mathbf{a_3} + \mathbf{b_3}t & T_{on} \le t < T_{on} + T_{f_c} \\ \mathbf{a_4} + \mathbf{b_4}t & T_{on} + T_{f_c} \le t < T \end{cases}$$

$$\mathbf{a_1} = 0 \quad \mathbf{b_1} = fs\frac{I_{L_k}}{T_{on_e}}$$

$$\mathbf{a_2} = (fl||fs)\left(I_{L_k} + \frac{A_k}{2} - \frac{T_{on_c} + 2T_{on_e}}{T_{on_c}}\right) + .. + fd\left(-I_{L_k}\frac{T_{on_e}}{T_{on_c}} - \frac{A_k}{2}\frac{T_{on_e}}{T_{on_c}}\right)$$

$$\mathbf{b_2} = (fl||fs)\frac{A_k}{T_{on_c}} + fd\left(\frac{I_{L_k}}{T_{on_c}} + \frac{A_k}{2T_{on_c}}\right)$$

$$\mathbf{a_3} = (fl||fd)\left(I_{L_k} + \frac{A_k}{2} + A_k\frac{T_{on}}{T_{f_c}}\right) + .. + fs\left[\frac{I_{L_k} + \frac{A_k}{2}}{T_{f_c}}(T_{on} + T_{f_c})\right]$$

$$\mathbf{b_3} = -(fl||fd)\left(\frac{A_k}{T_{f_c}}\right) - fs\left(\frac{I_{L_k} + \frac{A_k}{2}}{T_{f_c}}\right)$$

$$\mathbf{a_4} = fd\left[\frac{T}{T_{f_e}}\left(I_{L_k} - \frac{A_k}{2}\right)\right] \quad \mathbf{b_4} = -fd\left(\frac{I_{L_k - \frac{A_k}{2}}}{T_{f_e}}\right)$$

Fig. 6. $f(t, A_k, I_{L_k})$ linear segments definition.

Table 1
Evaluation of $f(t, A_k, I_{L_k})$

Inductor current $f_L(t, A_k, I_{L_k})$	Switch current $f_s(t, A_k, I_{L_k})$	Diode current $f_D(t, A_k, I_{L_k})$
$T_{on_e} = T_{f_e} = 0$	$T_{on_e} = T_{f_c} = T_i$	$T_{on_c} = T_{f_e} = T_i$
$T_{on_c} = T_{on}$	$T_{on_c} = T_{on} - T_i$	$T_{on_e} = T_{on} - T_i$
$T_{f_c} = T_f$	$T_{f_e} = T_f - T_i$	$T_{f_c} = T_f - T_i$
$f_l = 1$ $f_s = f_d = 0$	$f_s = 1$ $f_l = f_d = 0$	$f_d = 1$ $f_l = f_s = 0$

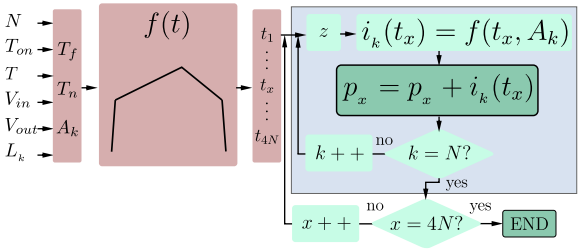

Fig. 7. Flow chart of characterization procedure.

$$i_{rms} = \sqrt{\frac{1}{T}\sum_{x=1}^{M}\left[\frac{m_x^2}{3}\left(t_{x+1}^3 - t_x^3\right) + m_x q_x\left(t_{x+1}^2 - t_x^2\right) + q_x(t_{x+1} - t_x)\right]} \tag{13}$$

Ripple rms value ($\widetilde{i}_{rms}$) has the same pattern as ripple amplitude. Thus, nulls for inductor current in operating points D_N exist when there is no inductance mismatch and they become local minimums when differences among inductors occur. Moreover switch and diode rms values have no cancellation points since no slope superposition exists, as expected.

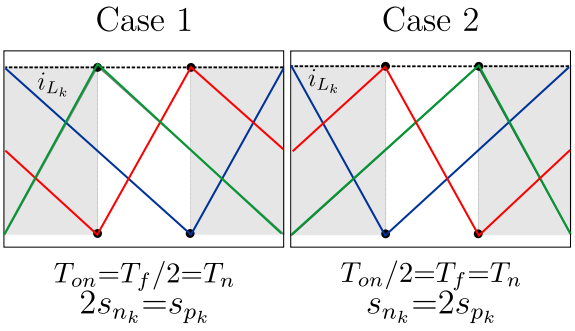

Fig. 8. Example of slopes superposition cases for i_{L_k}.

Table 2
Superposition cases ($N = 3$)

Case 1	Case 2
$T_{on} = T_f/2$	$T_{on}/2 = T_f$
$2T_{on} = (T - T_{on})$	$T_{on} = 2(T - T_{on})$
$3T_{on} = T$	$3T_{on} = 2T$
$T_{on}/T = 1/3$	$T_{on}/T = 2/3$

Table 3
Test bench parameters

Parameter	Value
f_{sw}	20kHz
V_{in}	20V
V_{out}	4V to 16V
$[L_1\ L_2\ L_3\ L_4\ L_5]$	[105.6 106 110.2 105.1 110.6] uH
$[R_{L1}\ R_{L2}\ R_{L3}\ R_{L4}\ R_{L5}]$	[22.5 23.3 21.5 23.8 21.8] mΩ

3.3. Harmonic content

The periodicity of the total current allows the computation of the discrete frequency components of the Fourier series as:

$$f(t) = \frac{a_0}{2} + \sum_{h=1}^{\infty}\left[\sqrt{a_h^2 + b_h^2}\ cos\left(\frac{2\pi h}{T}t - \theta_h\right)\right] \tag{14}$$

where $a_0/2$ is the dc value, $\sqrt{a_h^2 + b_h^2}$ is the amplitude of the h^{th} harmonic and θ_h is its phase angle. Considering that total currents can be segmented as linear functions, a_0, a_h and b_h can be calculated by computing the slope and intercept in each portion using the obtained inflexion points as:

$$a_0 = \frac{2}{T}\left[\sum_{x=1}^{3N}\int_{t_x}^{t_{x+1}}(m_x\tau + q_x)d\tau\right] \tag{15}$$

$$a_h = \frac{2}{T}\left[\sum_{x=1}^{3N}\int_{t_x}^{t_{x+1}}(m_x\tau + q_x)cos\left(\frac{2\pi h}{T}\tau\right)d\tau\right] \tag{16}$$

$$b_h = \frac{2}{T}\left[\sum_{x=1}^{3N}\int_{t_x}^{t_{x+1}}(m_x\tau + q_x)sin\left(\frac{2\pi h}{T}\tau\right)d\tau\right] \tag{17}$$

with m_x and q_x obtained with (12).

The existence of inductance mismatch gives rise to the appearance of harmonic content below the Nf_{sw} component; which is not present in the case of converters with the same phase inductances. Moreover, depending on the phases switching sequence, harmonic content of each component changes as presented in Antoszczuk et al. (2017). Therefore, evaluation of these components in the design stages, using the proposed

method, may be helpful in determining the filtering action and useful for cost functions in ripple optimization algorithms Antoszczuk et al. (2017).

4. Simulations and discussion

In order to show that the proposed characterization and its conclusions are correct, total current for all types of phase currents must be simulated and contrasted. Then, the simulation circuits consist on a 5-phase boost converter with input voltage $V_{in_{bst}} = 12$V, and a 5-phase buck converter with input voltage $V_{in_{bck}} = 45$V, period $T = 40\mu s$, $T_i = T/1000$, nominal inductor value $L_{nom} = 100\mu H$ and inductance tolerance of $\pm$ 7%. Then, the phase inductance values considered for the simulation are: $L_1 = 107$uH, $L_2 = 100$uH, $L_3 = 93$uH, $L_4 = 96$uH, $L_5 = 100$uH, with an associated resistance of 30mΩ. Duty cycles swept is performed keeping the same mean phase inductor current $I_{L_k} = 2.5$A for each case. Each phase and total currents are acquired from the simulated circuit, processed and compared with the characterized values.

Firstly, computed total current key points are compared with the information obtained by simulation so as to evaluate the method accuracy. In this sense, Fig. 9 exhibits i_{L_T} and i_{D_T} currents for the boost converter and i_{L_T} and i_{S_T} currents for a the buck converter for $D = 0.7$. The calculated p_x values are superimposed to the simulated waveforms. As it can be seen, the proposed method is able to correctly predict the key points value and location.

Moreover, in order to assess total ripple rms characteristic, rms curves are obtained using (11) and (13) and compared with rms values by conducting simulations for $D = 0.1 : 0.1 : 0.9$. Results for input and output total current for buck and boost converters are shown on Fig. 10 where computed rms curves are superimposed to the simulated values. Simulated values are obtained by running a converter simulation for each particular operation point, requiring a settling time to arrive at the steady state condition. As can be noted, rms value is accurately predicted in the evaluated range. Furthermore, it can be observed that, due to the inductance mismatch, the expected cancellation points in $\widetilde{i}_{L_{Trms}}$ turned into local minimums, whose values are also correctly predicted by the calculations.

Regarding switch current ripple rms value ($\widetilde{i}_{S_{Trms}}$) and diode current ripple rms value ($\widetilde{i}_{D_{Trms}}$), Fig. 10 shows the same pattern as the $\widetilde{i}_{L_{Trms}}$ of the respective topology but without the existence of nulls for the case with no inductance mismatch.

Finally, in order to evaluate harmonic content computation, i_{L_T} and i_{D_T} boost current ripples and i_{L_T} and i_{S_T} buck current ripples Fourier transforms were calculated using the proposed method, and then

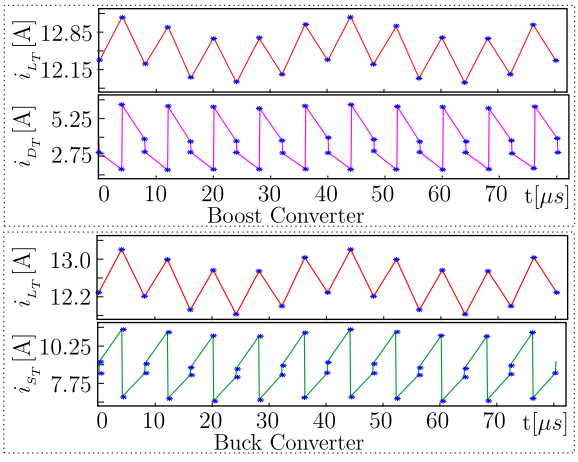

Fig. 9. i_{L_T}, i_{S_T} and i_{D_T} simulated currents (continuous line) and computed key points with the proposed characterization (dots).

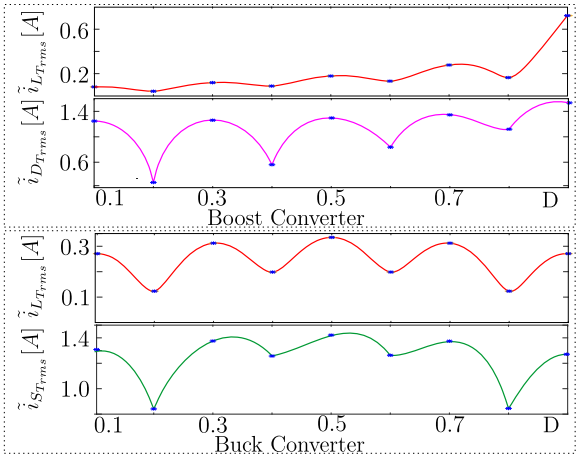

Fig. 10. $\widetilde{i}_{L_{Trms}}$, $\widetilde{i}_{S_{Trms}}$, $\widetilde{i}_{D_{Trms}}$ computed rms curves with the proposed characterization (continuous line) and rms values obtained by simulation (dots).

compared with the harmonics obtained from the simulated circuit. Moreover, two different switching sequences are presented in order to show that the characterization accurately computes the harmonics amplitude in both cases and could be useful when determining the best switching sequence using the methodology presented in Antoszczuk (2016). Each switching sequence is associated with a particular order in which the inductors are arranged. Fig. 11 shows the simulated and characterized harmonics for $D = 0.7$ with the switching sequence used in the computation of previous characteristics, which corresponds to inductors order [L_1 L_2 L_3 L_4 L_5].Fig. 12 shows the simulated and characterized harmonics components, for the same duty cycle with inductors order [L_3 L_1 L_4 L_2 L_5]. As expected, due to the inductance mismatch, no cancellation of the first $N-1$ harmonics exists. Moreover, it can be observed that harmonic content has changed significantly from one switching sequence to another, proving the importance of evaluating this ripple characteristic.

5. Experimental tests

The experimental tests aim at verifying that the proposed method and its conclusions can be applied in a real situation. The test set-up consists on a 5-phase buck converter ($N = 5$), shown on Fig. 13. Table 3 also shows the parameters of the converter and the value of the phase inductors, which result with a $\overline{L} = 107.5uH$ and a $\Delta L < \pm 3\%$. All measurements are performed considering a load of approximately 800 $m\Omega$, thus the duty cycle swept is carried out by changing the mean current reference. Output total current for different duty cycles is acquired, processed and compared with the characterized values.

The first test evaluates the proposed method accuracy for assessing total ripple inflexion points. In this sense, Fig. 14 exhibits the i_{L_T} and i_{L_k} waveforms for $D = 0.5$. The calculated p_{Lx} values are superimposed to measure total current. As it can be seen, the proposed method is able to correctly predict the inflexion points value and location. A zoomed in version of total inductor current is plotted in Fig. 15. As observed, total ripple amplitude results in $\Delta i_{L_T} = 0.5024A$, which is in accordance with the measured value $\Delta i_{L_T} = 0.51$, computing a 1.5% error. It must be pointed out that interpolation technique is used when computing total ripple amplitude for measured currents, in order to avoid errors introduced by switching noise.

Moreover, in order to assess the total output current ripple rms value, measurements are taken for output voltage range presented in Table 3. Results are shown in Fig. 16. As it can be seen, the proposed method is able to predict the rms value in the evaluated range. Furthermore, it can be observed that, due to the inductance mismatch, the expected $\widetilde{i}_{L_{Trms}}$

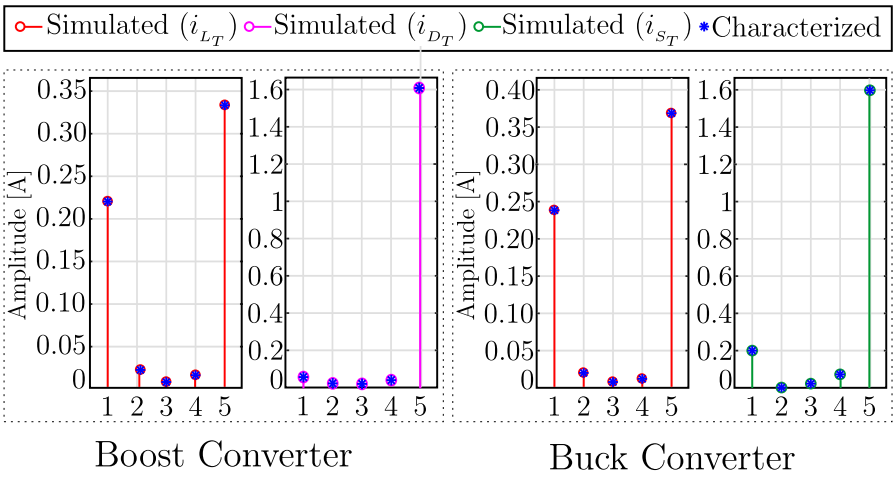

Fig. 11. i_{L_T}, i_{S_T} and i_{D_T} harmonics for $D = 0.7$.

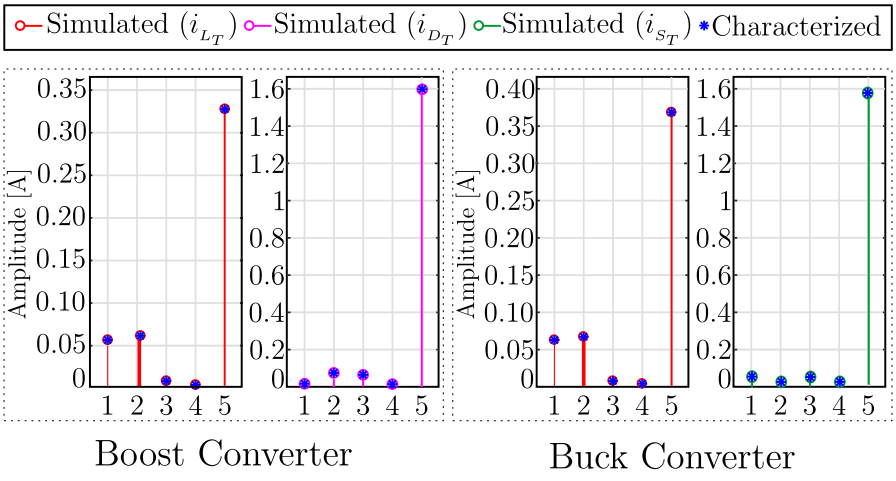

Fig. 12. i_{L_T}, i_{S_T} and i_{D_T} harmonics for $D = 0.7$ with a different switching sequence.

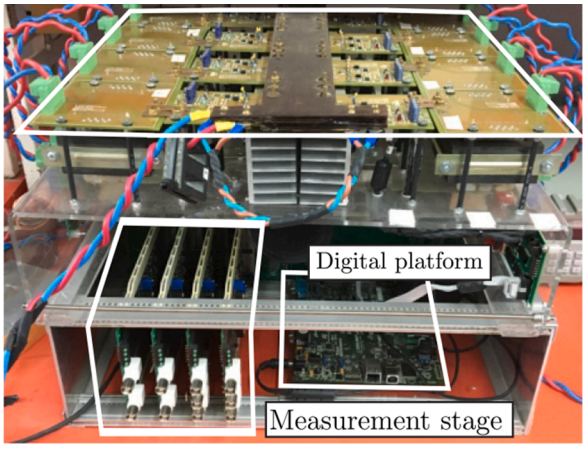

Fig. 13. Interleaved Buck converter test bench.

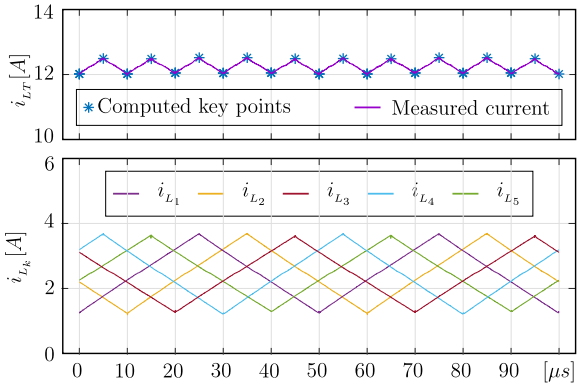

Fig. 14. Measured currents (continuous line) and computed inflexion points (dots).

cancellation points turned into local minimums, whose value was also correctly predicted by the calculations.

Finally, in order to evaluate the harmonic content, i_{L_T} Fourier transform was computed from the measured data points, and then compared with the harmonics calculated using the proposed method. Figure 17 shows the measured and characterized harmonics components, for $D = 0.3$ and $D = 0.7$. As expected, due to the inductance mismatch, no cancellation of the first $N - 1$ harmonics exists. The error between the calculated and measured $5f_{sw}$ components for $D = 0.3$ is 2% and for $D = 0.7$ is 1.45%. The observed errors can be attributed, in part, to the measurement process: for instance switching noise and ringing caused by capacitances and parasitic inductances (Fig. 15). Yet, each harmonic component proportion is correctly approximated, and

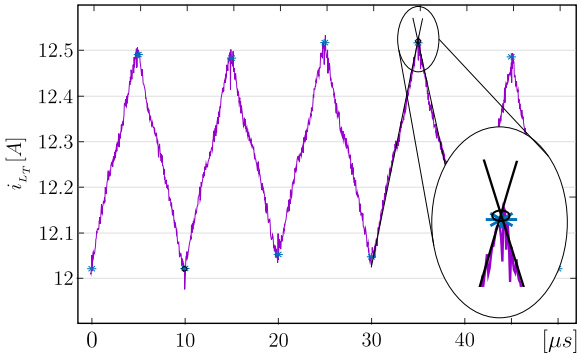

Fig. 15. Measured i_{LT} (continuous line) and computed inflexion points (dots). The zoomed-in detail shows the interpolation methodology.

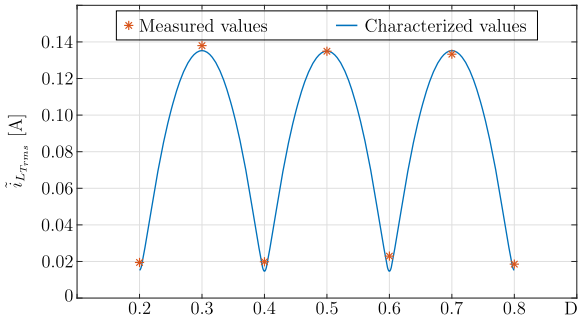

Fig. 16. Total inductor rms ripple value

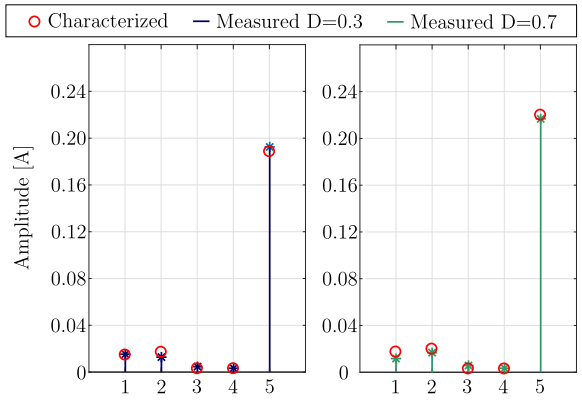

Fig. 17. i_{L_T} harmonics for $D = 0.3$ and $D = 0.7$.

therefore could be used to evaluate the inductance mismatch impact in a given design.

6. Conclusions

This paper presents a methodology that allows to obtain input and output total currents for several converter topologies operating in *BCM* and *CCM*, for any number of phases, any inductance ratio and operating points. With the obtained input and output currents it is possible to easily compute key characteristics such as ripple amplitude, currents rms value and harmonic content useful for converter analysis, design or optimization.

This methodology fills a gap in the literature by proposing a general waveform from which the phase currents in switches, diodes and inductors can be represented. Based on this representation, the proposed method only requires the value and location of certain key points in phase currents to compute the aforementioned characteristics. This computation avoids the need of performing numerous and extensive circuit simulations to evaluate different operating points in steady state conditions.

The experimental tests performed on a 5-phase buck converter demonstrated that the proposed method can be applied in real situation.

Declaration of Competing Interest

The authors declare that they have no known competing financial interests or personal relationships that could have appeared to influence the work reported in this paper.

Acknowledgments

This work was supported in part by the Universidad Nacional de Mar del Plata (UNMDP), the Consejo Nacional de Investigaciones Científicas y Tecnológicas (CONICET) PIP11220200102643CO and by the Agencia Nacional de Promoción Científica y Tecnológica (ANPCYT), Argentina.

References

Abu-Qahouq, J., Batarseh, M., Huang, L., & Batarseh, I. (2007). Analysis and small signal modeling of a non-uniform multiphase buck converter. *2007 IEEE Power Electron. Specialist Conf.*, 961–967. https://doi.org/10.1109/PESC.2007.4342118

Antoszczuk, P. (2016). Interleaved current control for multiphase converters with high dynamics mean current tracking. *IEEE Trans. Power Electron., 31*(12), 8422–8434. https://doi.org/10.1109/TPEL.2016.2517927

Antoszczuk, P., Cervellini, P., Retegui, R. G., & Funes, M. (2017). Optimized switching sequence for multiphase power converters under inductance mismatch. *IEEE Trans. Power Electron., 32*(3), 1697–1702. https://doi.org/10.1109/TPEL.2016.2602810

Antoszczuk, P. D., Retegui, R. G., Wassinger, N., Maestri, S., Funes, M., & Benedetti, M. (2014). Characterization of steady-state current ripple in interleaved power converters under inductance mismatches. *IEEE Trans. Power Electron., 29*(4), 1840–1849. https://doi.org/10.1109/TPEL.2013.2270005

Cervellini, P., Antoszczuk, P., Retegui, R. G., & Funes, M. (2020). Current ripple characterization in dcm interleaved power converters under inductance mismatch. *IEEE Trans. Circuits Syst. II Express Briefs, 67*(7), 1269–1273. https://doi.org/10.1109/TCSII.2019.2928995

Farahani, M., Shamsi-nejad, M. A., & Najafi, H. R. (2020). Design and construction of a digital solar array simulator with fast dynamics and high performance. *Sol. Energy, 196*(2019), 319–326. https://doi.org/10.1016/j.solener.2019.12.032

Foley, R. F., Kavanagh, R. C., & Egan, M. G. (2012). Sensorless current estimation and sharing in multiphase buck converters. *IEEE Trans. on Power Electron., 27*(6), 2936–2946. https://doi.org/10.1109/TPEL.2010.2042072

Galigekere, V. P., & Kazimierczuk, M. K. (2012). Analysis of pwm z-source dc-dc converter in ccm for steady state. *IEEE Trans. Circuits Syst. I Regul. Pap., 59*(4), 854–863. https://doi.org/10.1109/TCSI.2011.2169742

García, O., Zumel, P., de Castro, A., & Cobos, J.a. (2006). Automotive dc-dc bidirectional converter made with many interleaved buck stages. *IEEE Trans. Power Electron., 21*(3), 578–586. https://doi.org/10.1109/TPEL.2006.872379

Garca, O., de Castro, A., Zumelis, P., & Cobos, J. A. (2007). Digital-control-based solution to the effect of nonidealities of the inductors in multiphase converters. *IEEE Trans. Power Electron., 22*(6), 2155–2163. https://doi.org/10.1109/TPEL.2007.909406

Gu, Y., & Zhang, D. (2013). Interleaved boost converter with ripple cancellation network. *IEEE Trans. Power Electron., 28*(8), 3860–3869. https://doi.org/10.1109/TPEL.2012.2228505

Gupta, P., & Patra, A. (2005). Hybrid mode-switched control of dc-dc boost converter circuits. *IEEE Trans. Circuits Syst. II Express Briefs, 52*(11), 734–738. https://doi.org/10.1109/TCSII.2005.852189

Huangfu, Y., Ma, Y., Bai, H., Xu, L., Wang, A., & Ma, R. (2021). A family of high gain fuel cell front-end converters with low input current ripple for pemfc power conditioning systems. *Int. J. Hydrog. Energy., 46*(53), 27156–27172. https://doi.org/10.1016/j.ijhydene.2021.05.174

Huber, L., Irving, B. T., & Jovanovic, M. M. (2008). Open-loop control methods for interleaved dcm/ccm boundary boost pfc converters. *IEEE Trans. Power Electron., 23*(4), 1649–1657. https://doi.org/10.1109/TPEL.2008.924611

Johnson, B., & Krein, P. (2017). An analytical time–domain expression for the net ripple produced by parallel interleaved converters. *IEEE Trans. Circuits Syst. II Express Briefs, 64*(3), 289–293. https://doi.org/10.1109/TCSII.2016.2557620

Karatzaferis, I., Tatakis, E. C., & Papanikolaou, N. (2017). Investigation of energy savings on industrial motor drives using bidirectional converters. *IEEE Access, 5*, 17952–17961. https://doi.org/10.1109/ACCESS.2017.2748621

Kjaer, S. B., Pedersen, J. K., & Blaabjerg, F. (2005). A review of single-phase grid-connected inverters for photovoltaic modules. *IEEE Trans. Ind. Appl., 41*(5), 1292–1306. https://doi.org/10.1109/TIA.2005.853371

Liu, H., Zhang, D., & Wang, D. (2017). Design considerations for output capacitance under inductance mismatches in multiphase buck converters. *IEEE Trans. Power Electron., 32*(7), 5004–5015. https://doi.org/10.1109/TPEL.2016.2605700

Liu, Z., Xu, Z., & Zhang, X. (2021). A novel real-time fast fault-tolerance diagnosis and fault adjustment strategy for m-phase interleaved boost converter. *IEEE Access, 9*, 11776–11786. https://doi.org/10.1109/ACCESS.2021.3050705

Mihajlovic, Z., & and, B. L. (2004). Output ripple analysis of switching dc-dc converters. *IEEE Trans. Circuits Syst. I Regul. Pap., 51*(8), 1596–1611. https://doi.org/10.1109/TCSI.2004.832792

Monmasson, E., Idkhajine, L., Cirstea, M. N., Bahri, I., Tisan, A., & Naouar, M. W. (2011). Fpgas in industrial control applications. *IEEE Trans. Industr. Inform., 7*(2), 224–243. https://doi.org/10.1109/TII.2011.2123908

Nouri, T., Babaei, E., & Hosseini, S. H. (2013). A generalized ultra step-up DC-DC converter for high voltage application with design considerations,electr. *Power Syst. Res., 105*, 71–84. https://doi.org/10.1016/j.epsr.2013.07.012

Rodriguez, E., El Aroudi, A., Guinjoan, F., & Alarcon, E. (2012). A ripple-based design-oriented approach for predicting fast-scale instability in dc-dc switching power supplies. *IEEE Trans. Circuits Syst. I Regul. Pap., 59*(1), 215–227. https://doi.org/10.1109/TCSI.2011.2161396

Schuck, M., & Pilawa-Podgurski, R. C. N. (2015). Ripple minimization through harmonic elimination in asymmetric interleaved multiphase dc converters. *IEEE Trans. Power Electron., 30*(12), 7202–7214. https://doi.org/10.1109/TPEL.2015.2393812

Seyezhai, R., & Mathur, B. L. (2012). Design and implementation of interleaved boost converter for fuel cell systems. *Int. J. Hydrogen Energy, 37*(4), 3897–3903. https://doi.org/10.1016/j.ijhydene.2011.09.082

Slah, F., Mansour, A., Hajer, M., & Faouzi, B. (2017). Analysis, modeling and implementation of an interleaved boost DC-DC converter for fuel cell used in electric vehicle. *Int. J. Hydrogen Energy, 42*(48), 28852–28864. https://doi.org/10.1016/j.ijhydene.2017.08.068

Tsolaridis, G., Jeong, M., & Biela, J. (2021). Evaluation of current control structures for multi-phase interleaved dc-dc converters. *IEEE Access, 9*, 142616–142631. https://doi.org/10.1109/ACCESS.2021.3121060

Valdez-Resendiz, J., Rosas-Caro, J., Mayo-Maldonado, J., & Calderon-Zavala, G. (2018). Input-current/output-voltage ripple mitigation in the double dual boost converter. *Electr. Power Syst. Res., 162*, 150–160. https://doi.org/10.1016/j.epsr.2018.05.013

Wang, X., Zhao, Z., Li, K., Chen, K., & Liu, F. (2019). Analysis of the steady-state current ripple in multileg class-d power amplifiers under inductance mismatches. *IEEE Trans. Power Electron., 34*(4), 3646–3657. https://doi.org/10.1109/TPEL.2018.2850913